Effect of Soft-Segment CH_2/O Ratio on Morphology and Properties of a Series of Polyurethane Elastomers

DARREN J. MARTIN,[1,*] GORDON F. MEIJS,[2] GORDON M. RENWICK,[1] PATHIRAJA A. GUNATILLAKE,[2] and SIMON J. McCARTHY[2]

The Cooperative Research Centre (CRC) for Cardiac Technology: [1]Department of Materials Science, University of Technology, Sydney, Broadway, NSW 2007, Australia; [2]CSIRO Division of Chemicals and Polymers, Private Bag 10, Rosebank MDC, VIC 3169, Australia

SYNOPSIS

A series of six thermoplastic polyurethane elastomers were synthesized from a 4,4′-methylene diphenyl diisocyanate (MDI) and 1,4-butanediol (BDO) chain extender, with poly(ethylene oxide) (PEO), poly(tetramethylene oxide) (PTMO), poly(hexamethylene oxide) (PHMO), poly(octamethylene oxide) (POMO), poly(decamethylene oxide) (PDMO), and poly(1,6-hexyl carbonate)diol (PCDO) macrodiol soft segments. The soft-segment molecular weights employed were similar (approximately 1000 g/mol) and each polyurethane contained 55% (w/w) of the soft-segment macrodiol. Differential scanning calorimetry (DSC), dynamic mechanical thermal analysis (DMTA), wide-angle X-ray diffraction (WAXD), and Fourier transform infrared spectroscopy (FTIR) techniques were employed to characterize the morphology. Tensile and Shore hardness tests were also performed. Materials were tested in the as-molded, solvent-cast, and annealed states. It was found that the polyurethanes produced from macrodiols with the highest CH_2/O ratio displayed greater hard-domain crystallinity, a higher degree of phase separation, and the greatest hardness, stiffness, and opacity. POMO- and PDMO-based polymers displayed evidence of paracrystallinity in the soft domains. The PCDO-based material displayed a higher degree of phase mixing compared to the polyether-based materials. Annealing increased hard-domain crystallinity in all the polyether-based materials. The solvent-cast POMO- and PDMO-based materials had poor mechanical properties and were difficult to cast. The materials containing macrodiols with the lowest CH_2/O ratio were more readily solvent-cast and produced strong, useful films. Morphologies of the solvent-cast materials differed greatly from those of the molded materials.

INTRODUCTION

Polyurethane elastomers are linear segmented copolymers with an $[HS]_n$-type structure. Typically, these materials consist of a relatively flexible component called the soft segment (S) and a relatively polar and stiff component known as the hard segment (H). In the solid state, unique elastomeric properties are observed due to microdomain formation. The so-called hard domains provide both physical crosslink sites and fillerlike reinforcement to the soft-segment matrix. At higher temperatures, a homogeneous melt can be formed, allowing the material to be thermally processed.

Schematic Thermoplastic Polyurethane Chain Section

An understanding of morphology is critical to the rational design of improved polyurethanes. Morphological factors such as degree of hard/soft-phase

* To whom correspondence should be addressed.

Journal of Applied Polymer Science, Vol. 60, 557–571 (1996)
 CCC 0021-8995/96/040557-15

separation, crystallinity, and domain size influence properties such as hardness, stiffness, tensile strength, and clarity.

The morphology and properties of thermoplastic polyurethane elastomers are greatly influenced by the compatibility of starting compounds,[1,2] the ratio of hard- and soft-block components,[3-5] the average block lengths employed (including molecular weight distribution),[3,4,6-8] the thermal history of the material,[9-12] and the mechanical history endured by the material.[13,14]

The relative polarities (solubility parameters) of hard- and soft-block components influences the microstructure of the material produced. Ophir and Wilkes[1] studied the degree of phase separation and interfacial thickness for polyester-based and polyether-based materials using small-angle X-ray scattering. They concluded that polyester-based polyurethanes (with stronger interactions present between soft and hard segments) displayed broader transition zones than did polyether-based polymers.

Hard-segment content significantly affects physical properties such as hardness, the Young's modulus, and tear strength. Also, the performance of polyurethane elastomers at elevated temperatures is very dependent upon the structure of the rigid segments and their ability to remain coherent at higher temperatures.

Ng et al.[6] employed dynamic mechanical thermal analysis (DMTA) and differential scanning calorimetry (DSC) methods to characterize several linear segmented polyurethanes of well-defined hard- and soft-block molecular weights and molecular weight distributions. They reported that the materials containing a monodisperse distribution of hard-segment lengths displayed sharper, more pronounced high-temperature DSC endotherms associated with more effective packing of equilength hard blocks into microcrystalline domains. Chen et al. showed that for a fixed hard/soft composition ratio increasing the hard- and soft-segment lengths provides more complete phase separation, an increase in modulus, and a decrease in soft domain T_g (due to a purer soft phase).[7]

Thermal analysis and small-angle X-ray scattering (SAXS) studies[11,12] have shown that the morphology of these materials can be strongly influenced by aging and/or annealing. Recently, Li et al.[2] reported on how the system viscosity, hard-segment mobility, and strength of hard-segment interactions were important in governing microstructures and morphological kinetics in segmented polyurethanes.

The rate of change of morphology was studied by several workers.[15-20] In 1993, Bras et al.[18] carried out simultaneous, time-resolved SAXS and wide-angle X-ray diffraction (WAXD) experiments on a polyurethane elastomer during an annealing treatment. They were able to show the rate of development of both hard-domain crystallinity and of a microdomain structure.

In this article, we report on the effects of changing the chemistry of the soft-block component on morphology and physical properties and compare how each formulation is affected by method of fabrication (i.e., solvent casting vs. compression molding) and by subsequent annealing. The pure macrodiols and a 4,4′-methylene diphenyl diisocyanate/1,4-butanediol (MDI/BDO) copolymer were also characterized to facilitate the interpretation of some of the morphological features.

EXPERIMENTAL

Materials and Synthesis

All six polyurethanes (PUs) included hard segments comprising MDI and BDO and a macrodiol weight percent of 55%. The polyether macrodiols employed had the following general structure:

$$HO-[(CH_2)_m-O-]_n-H$$

where m = 2, 4, 6, 8, and 10 for poly(ethylene oxide) (PEO), poly(tetramethylene oxide) (PTMO), poly(hexamethylene oxide) (PHMO), poly(octamethylene oxide) (POMO), and poly(decamethylene oxide) (PDMO), respectively. The other macrodiol employed was poly(1,6-hexyl carbonate)diol:

$$HO-[(CH_2)_6-O-\overset{\overset{O}{\|}}{C}-O-]_n-H$$

The PHMO, POMO, and PDMO macrodiols were synthesized by condensation polymerization of hexane, octane, and decane diols.[19] The PEO (Aldrich), PTMO (Aldrich), and poly(1,6-hexyl carbonate)diol (PCDO) (Polysciences) materials were commercially available. The hydroxyl numbers of all macrodiols were determined by a standard procedure (ASTM D2849-method C). The MDI and BDO were distilled and degassed, respectively, and all polyols were dried thoroughly under a vacuum of better than 0.1 Torr at 105°C for at least 12 h prior to synthesis.

Synthesis of the PUs involved a two-step bulk polymerization. MDI was weighed into a reaction flask fitted with a condenser, stirrer, nitrogen inlet,

and an addition funnel. The reaction flask was placed into an oil bath at 80°C and the molten, dried macrodiol was then added slowly from the addition funnel over a period of 10 min and reacted for a total time of 2 h while stirring. BDO was then added to the prepolymer from a syringe and stirred at high speed for 2 min. The polymer was then poured onto a glass-reinforced Teflon sheet and cured at 100°C for 4 h under dry nitrogen.

The copolymer consisting purely of MDI/BDO hard segment was synthesized by solution polymerization. An adaptation of the Lyman synthesis method[20] was employed, where 1,4-butanediol replaced ethylene glycol. The solvent used was a 50/50 mixture of dimethyl sulfoxide and 4-methyl-2-pentanone.

The as-synthesized PUs were compression-molded into 1.3 mm-thick plaques at temperatures of 185–190°C using a water-cooled hydraulic press (DSC thermograms of the as-synthesized materials revealed that they were all completely molten in this range). The cooling procedure was kept uniform for all materials by carefully controlling the water flow rate. The MDI/BDO hard-segment polymer was dried and compression-molded in a similar manner as the PU samples, except that a molding temperature of 240°C was employed. Annealing was carried out on predried samples (0.1 Torr at 40°C overnight) under a dry nitrogen purge at 150 and 120°C for 10 and 24 h, respectively. Annealed samples were allowed to cool to room temperature slowly in the oven. Solvent-casting was carried out from 10% w/v solutions in dimethylformamide. These polymers were cast into a solid Teflon mold held at 50°C under a steady flow of dry nitrogen. Complete films were then dried (0.1 Torr at 40°C overnight) prior to analysis.

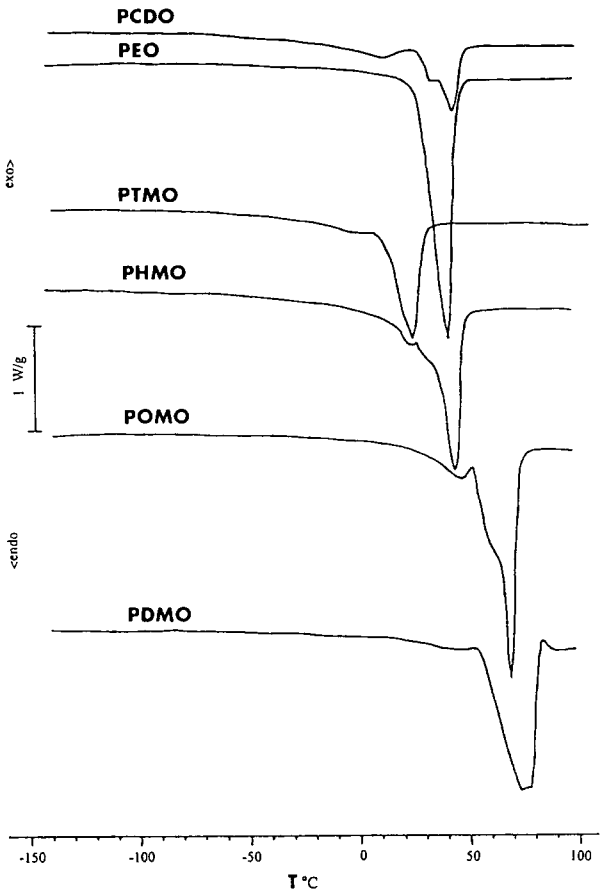

Figure 1 DSC thermograms for the pure macrodiols.

Instrumentation and Methods

Molecular weight analysis of the as-molded materials was carried out on a Spectra Physics GPC sys-

Table I Raw Material Molecular Weights and Thermal Transitions

Material	Molecular Weight/g mol^{-1}	T_m (°C)	ΔH_f (Jg^{-1})	T_g (°C)
PEO	987[a]	38	154.7	−72
PTMO	1014[a]	23	109.5	−96
PHMO	988[a]	42	132.8	−35
POMO	947[a]	67	168.0	−24
PDMO	875[a]	70	183.0	−25
PCDO	893[a]	41	62.5	−68
MDI/BDO[c]	41,000[b]	180–240[d]	51.1[e]	80[f]

[a] Via hydroxyl number determination.
[b] Via GPC calibrated against PS standards; M_n = 41,000; M_w = 73,000.
[c] Pure hard block polymer.
[d] Range for melting. Actual T_m values depended strongly on thermal history.
[e] ΔH value for MDI/BDO material annealed at 210°C for 3 h.
[f] T_g value for MDI/BDO material in the as-molded condition.

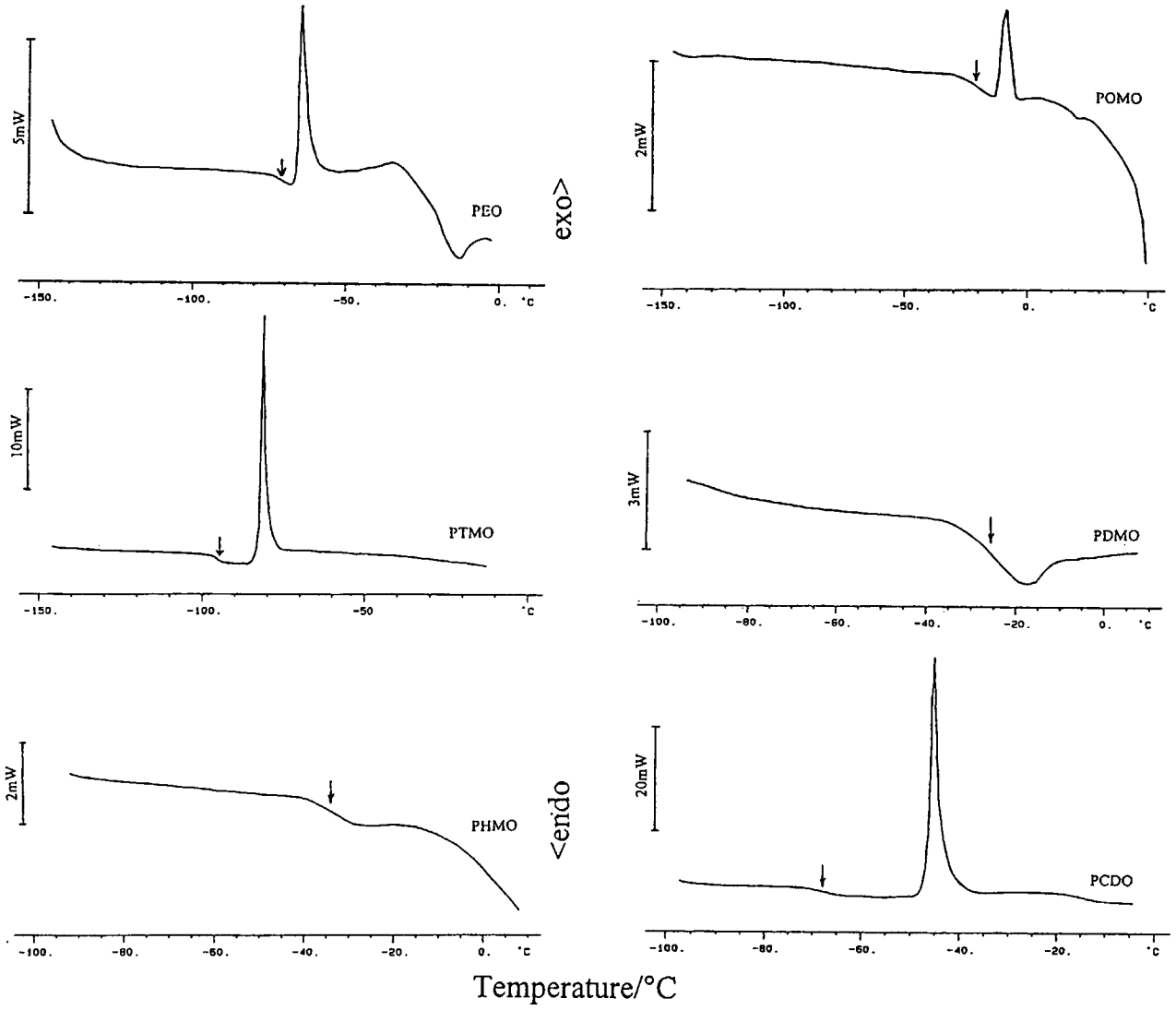

Figure 2 DSC thermograms for rapidly quenched macrodiols. Arrows indicate glass transitions.

tem using dimethylformamide containing 0.05*M* LiBr as the mobile phase. Columns of pore size 10^2, 10^3, and 10^5 Å were employed, and the system was calibrated against six polystyrene standards. DSC measurements were performed on a Mettler DSC30 with a 10°C/min heating rate. DSC samples were dried (0.1 Torr at 40°C overnight) prior to testing, and a sample weight of about 10 mg was used. Dynamic mechanical testing was carried out on a Polymer Laboratories DMTA equipped with tensile head and reducing force option, with a heating rate of 2°C/min and frequency setting of 2 Hz.

WAXD work was carried out on a Siemens D5000 diffractometer using CuKα radiation. Transmission Fourier transform infrared spectroscopy (FTIR) spectroscopy was done on a Bio-Rad FTS-7 spectrometer. Thin-film samples were pressed at 200°C between microscope slides, one of which was coated with a thin film of "Freekote 700-NC" (Dexter Corp.) mold release agent; the other was lined with a thin film of FEP to facilitate easy sample recovery. The pressed films were allowed to cool in air prior to annealing at 120°C for 24 h and were not detached from the glass slides until after annealing to prevent reversion or shrinkage. Films were kept in a vacuum oven up until the time of testing, and spectra were obtained under a dry nitrogen purge to minimize the effects of water vapor.

Tensile testing was carried out on five replicates of each material with an Instron model 4032 universal testing machine. Smaller-than-standard tensile dumbbell samples were punched from the molded sheet stock. The smaller samples (t = 1.3

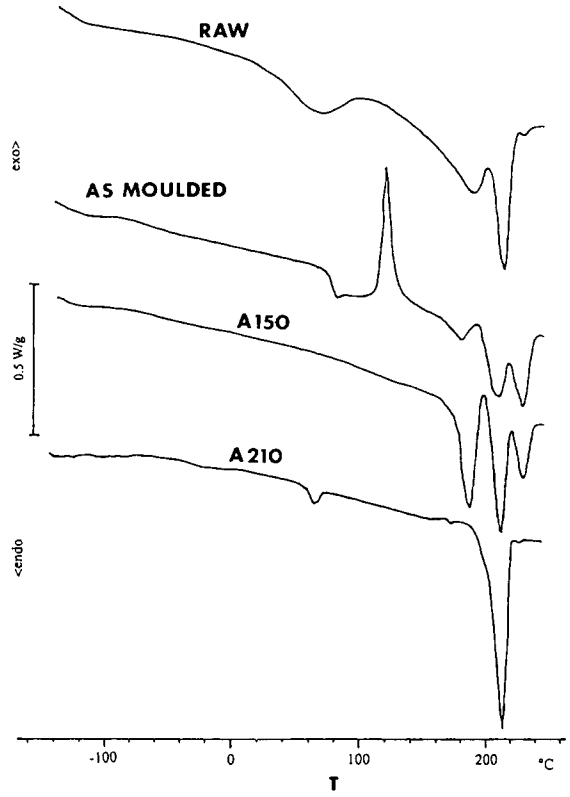

Figure 3 DSC thermograms for the MDI/BDO (hard segment only) polymer.

mm, w = 4.3 mm, l = 30 mm) were required to allow for large elongation behavior and to enable a comparison with previous tensile results involving *in vivo* and *in vitro* degradation studies,[21-23] which employed the same-sized dumbbell samples. A 1 kN load cell was used and the crosshead speed was 500 mm/min. Gauge lengths of 20 mm were used, and pneumatic grips were required to hold the test specimens. Shore hardness values were measured at 20°C with calibrated A and D scale indentors by stacking five 1.3 mm-thick moldings together on a flat surface.

RESULTS AND DISCUSSION

Raw Materials Characterization

Table I shows the molecular weight, melting temperature, enthalpy of fusion, and glass transition temperature values of the pure macrodiols and the MDI/BDO copolymer. The macrodiols are very crystalline in their pure state as evidenced by the DSC and WAXD results (Figs. 1 and 4). Polyol T_g values were obtained by quenching molten and dried material in liquid nitrogen prior to DSC analysis. T_g values were taken as the midpoints of inflectional tangents drawn through the greatest slope during the transition and intersecting extrapolated base lines.

Figure 1 shows the DSC curves for the dried pure polyols while Figure 2 shows the thermograms for the dried, melted, then rapidly cooled polyols. As the number of methylene groups in the polyether repeat unit is increased from 4 to 10, there is an accompanying increase in melting temperature. PEO is an exception and melts at a temperature between that of PTMO and PHMO. Glass transition temperatures of the polyols (indicated by small arrows) also show a similar trend. Some of the thermograms of the rapidly quenched polyols (for PEO, PTMO, POMO, and PCDO) show sharp cold crystallization exotherms following T_g. Evidence of condensation which formed on the outer surface of the sample pans during transfer from liquid nitrogen to the DSC cell can be seen for the PEO, PHMO, and POMO runs.

Figure 3 shows DSC traces for the MDI/BDO pure hard-segment material following varying thermal treatments. Compression molding of this polymer involved comparatively fast cooling from the melt; hence, the as-molded sample displayed quite

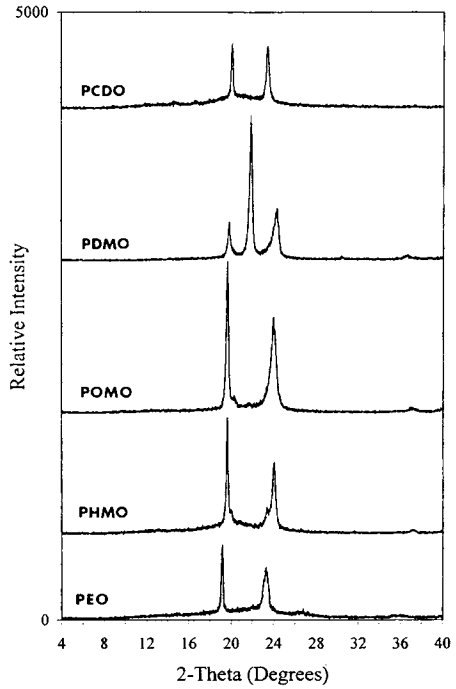

Figure 4 WAXD patterns for the pure macrodiols excluding PTMO which was partially molten at room temperature.

Table II WAXD Peak Positions for Raw Materials

Material	Diffraction Angles, 2θ	d-spacings (Å)
PEO	19.14, 23.35	4.63, 3.81
PHMO	19.64, 24.11	4.52, 3.69
POMO	19.64, 23.98	4.52, 3.71
PDMO	19.77, 21.84, 24.29	4.49, 4.07, 3.66
PCDO	20.08, 23.41	4.42, 3.80
MDI/BDO (Annealed 210 deg)	16.31, 18.01, 22.91, 25.24	5.43, 4.92, 3.88, 3.53

a prominent T_g at 80°C since some regions did not have sufficient time to crystallize. This curve also includes a "cold crystallization" exotherm. Multiple melting endotherms are observed in these thermograms, indicating the presence of regions of varying degrees of order. Annealing at 210°C for 3 h produced a single high-temperature endotherm at 215°C, indicating that a material predominantly composing the more highly ordered structure is attainable.

Figure 4 shows the WAXD patterns for all pure macrodiols apart from PTMO, which was partially molten at room temperature and unsuitable for testing. The very sharp diffraction peaks indicate the presence of a repeating unit cell structure in all of the waxy materials. The differing peak positions indicate differing unit cell dimensions brought about by variations in the packing ability of each material. Table II includes WAXD angles and d-spacing values for the pure macrodiols and MDI/BDO polymer as calculated by the Bragg equation.

Figure 5 shows the WAXD patterns for the MDI/BDO polymer after molding and annealing treatments. Unlike the polyols, the hard material does not display very sharp peaks (note the relative intensity scale differences).

Annealing does produce a broad "diffraction halo," and the diffraction pattern for the sample annealed at 210°C also shows some small peaks, possibly indicating some form of crystallinity. It is likely that the size of any crystals present is considerably less than 1000 Å. This can cause diffraction

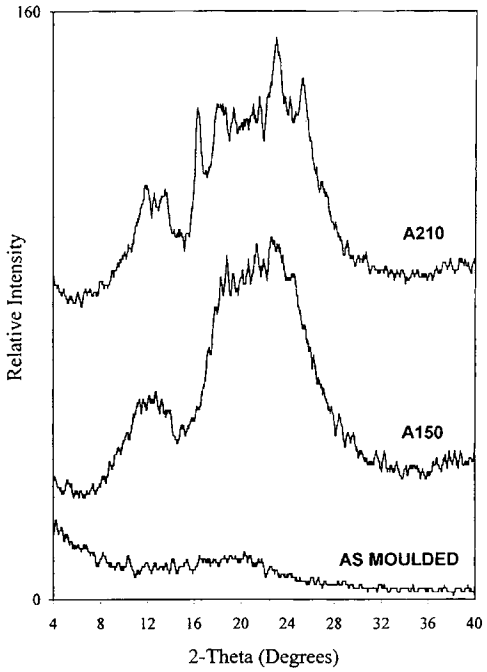

Figure 5 WAXD patterns for the MDI/BDO polymer in the as-molded and annealed states.

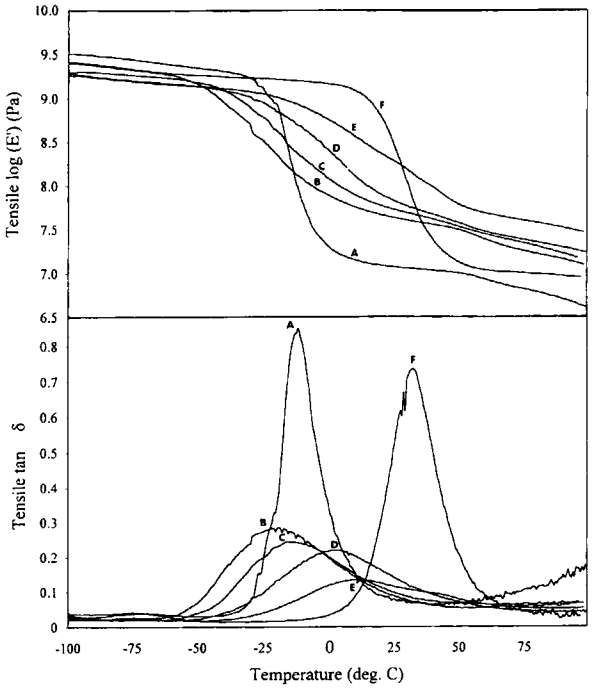

Figure 6 DMTA curves for (A) 2M, (B) 4M, (C) 6M, (D) 8M, (E) 10M, and (F) PCM.

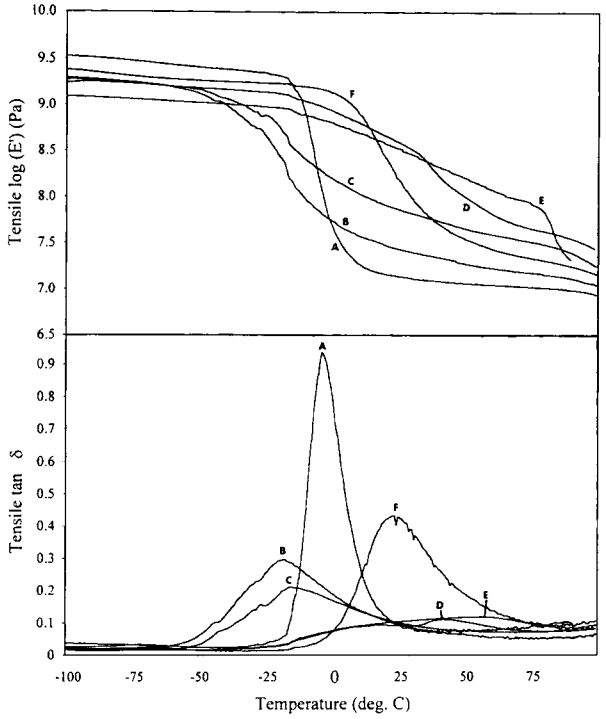

Figure 7 DMTA curves for (A) 2SC, (B) 4SC, (C) 6SC, (D) 8SC, (E) 10SC, and (F) PCSC.

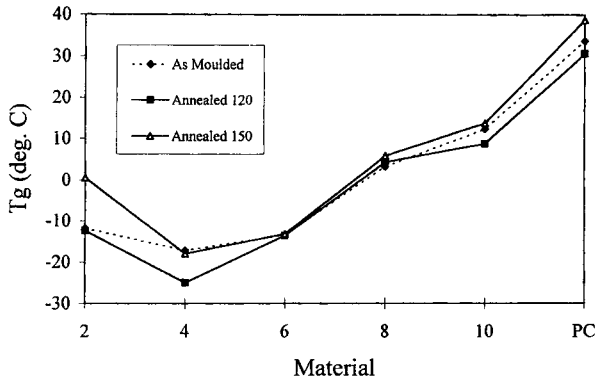

Figure 8 Variations in polymer T_g with annealing.

peak broadening and must be taken into consideration.[24] Three of the observed peak positions (d = 4.92, 3.88, and 3.53 Å) compare favorably with those quoted for other crystalline MDI/BDO-based PUs and MDI/BDO model compounds.[3,25-28] The 5.43 Å peak is not due to MDI/BDO crystallites and has been attributed to ordering which occurs between "single MDI" sequences. This phenomenon will be tested and discussed in later publications. The MDI/BDO polymer in this study involved a relatively high molecular weight and broad molecular weight distribution when compared to other, shorter model compounds seen in the literature; hence, it possessed a high viscosity and poorer "crystallizability." The diffraction patterns suggest a randomly folded or "paracrystalline" morphology, i.e., lacking a continuous repeating lattice framework. This type of structure has been suggested by Koberstein and Stein[29] in their model for PU morphology.

Strong support for chain folding of hard-segment sequences in hard-segment model compounds was presented by Camberlin et al.[30] They took measurements of melting temperatures of MDI/BDO hard-segment analogs as a function of sequence length. These measurements showed a maximum melting temperature at three MDI units per sequence (208°C). This decrease in T_m above three units was attributed to the incorporation of defects in the crystal structure due to the occurrence of chain folding.

Table III PU T_g Values vs. Pure Soft-segment T_g Values and the Effects of Annealing on PU T_g Values

	PU T_g Values (°C) via DMTA (Thermal History)			
Material	(M)[a]	(A120/24)[b]	(A150/10)[c]	ΔT_g[d]
2	−11.8	−12.4	0.5	60.2
4	−17.2	−25.0	−18.0	78.8
6	−13.4	−12.4	−13.2	21.6
8	3.3	4.4	5.9	27.3
10	12.3	8.8	13.7	37.3
PC	33.7	30.6	38.7	101.7

[a] As molded condition.
[b] Annealed at 120°C for 24 h.
[c] Annealed at 150°C for 10 h.
[d] ΔT_g = (T_g of as-molded PU) − (T_g of pure soft segment [Table I]).

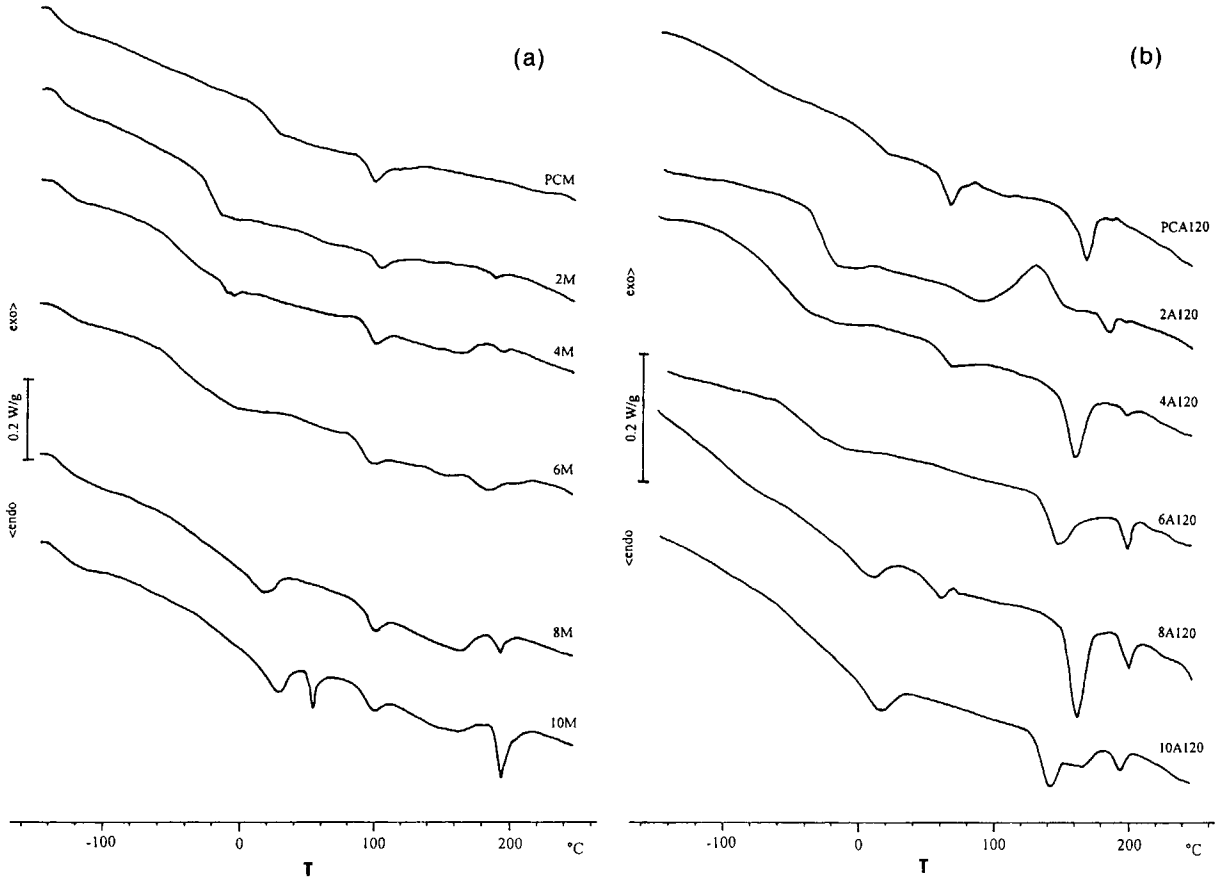

Figure 9 (a) DSC thermograms for the as-molded polyurethanes; (b) DSC thermograms for the PUs annealed at 120°C for 24 h; (c) DSC thermograms for the PUs annealed at 150°C for 10 h; (d) DSC thermograms for the solvent-cast PUs.

The structure described above is more likely to yield multiple endothermic behavior in DSC thermograms due to the variability in available packing conformations. These results show that in DSC annealing studies the behavior of the pure MDI/BDO material is very similar to that observed for the microphase separated hard domains in MDI/BDO-based PUs. The results for these single hard- and soft-block component materials have become very important when analyzing the PUs themselves.

POLYURETHANE SERIES

Nomenclature Employed

The nomenclature used for this series is of the form *XY###*, where *X* equals the number of methylene groups contained in the repeat unit of the polyether soft segment employed (or PC in the case of the PCDO soft segment) and *Y* represents an abbreviation of the fabrication method (*M* = as-molded, A = molded and annealed, and SC = solvent cast). If the sample has been annealed, this is also followed by the annealing temperature. For example, 4A120 is a PTMO-based material that was molded and subsequently annealed at 120°C for 24 h. PCSC represents a PCDO-based material fabricated by solvent casting.

Dynamic Mechanical Behavior

Figure 6 illustrates the dynamic mechanical behavior of each as-molded material. The storage modulus (E') vs. temperature plot shows a drop in stiffness for each material accompanying the soft-domain glass transition. At room temperature, an increase in the soft-segment CH_2/O ratio is accompanied by an increase in stiffness, with PCM having the highest storage modulus. The tan δ vs. temperature curves display loss peaks associated with the glass transition and damping capacity of the soft domains. An additional small shoulder seen at approximately

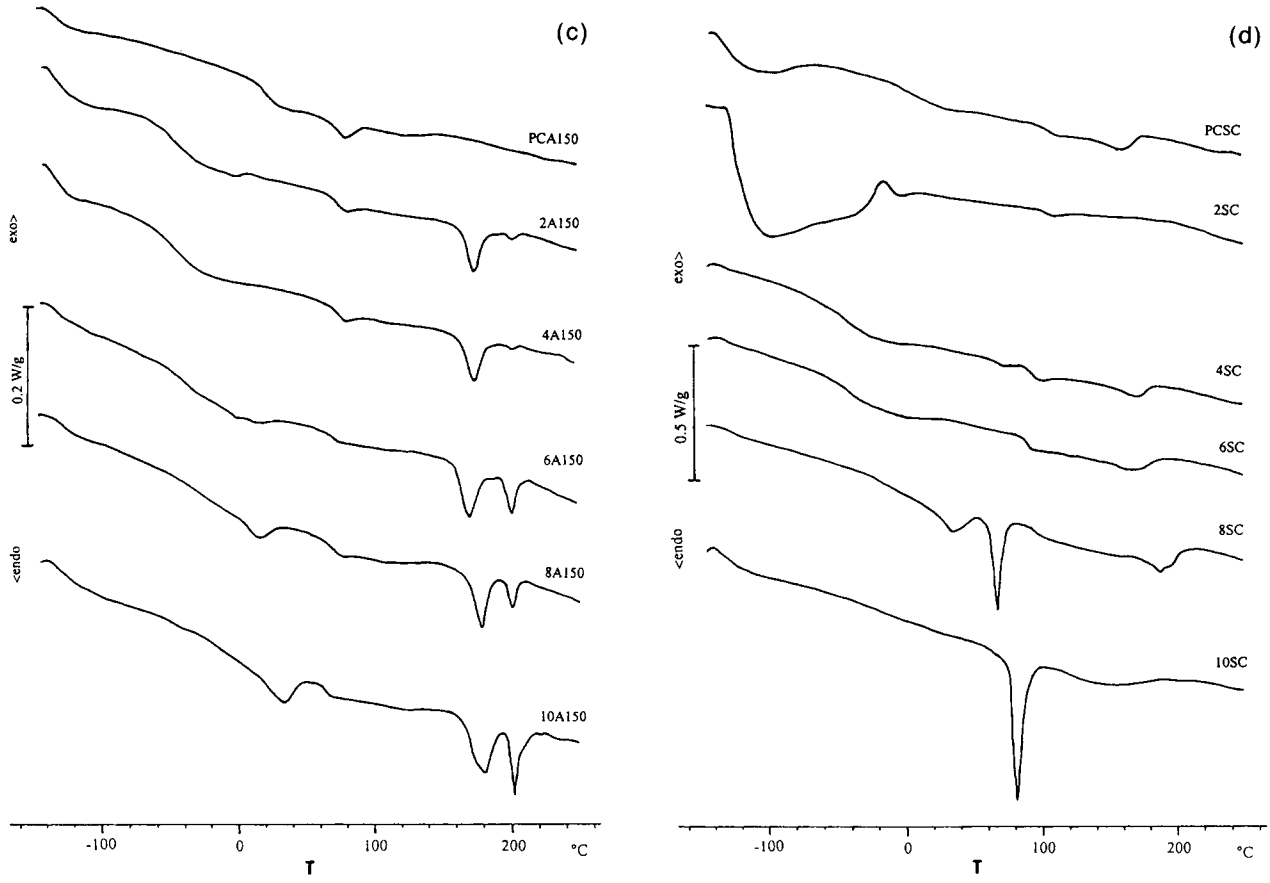

Figure 9 (*Continued from the previous page*)

45°C for 10M may be due to the melting of paracrystalline PDMO soft segments. The sharpness and height of the damping peaks give information about the degree of order and the freedom of motion of molecules in the soft domains. PCM and 2M display the most prominent damping peaks, suggesting that they are more amorphous than are the other materials. The fact that they were the only completely transparent materials supports this argument. A flattening and broadening of the loss peaks occurs as higher CH_2/O ratio soft segments are employed. Incorporation of more of the flexible ether linkages could improve damping. Also, the degree of crystallinity of the soft domains increases as the CH_2/O ratio increases (as shown by DSC). The presence of crystallites is known to have an inhibiting effect on molecular motion in the amorphous regions—hence, a broadening and flattening effect on DMTA loss peaks (especially in 8M and 10M).[31,32]

The DMTA curves for the annealed materials showed very similar features to those of the as-molded materials. Damping peak shifts are listed in Table III. Figure 7 shows the DMTA curves for the solvent-cast films. 2SC, 4SC, 6SC, and PCSC behave similarly to their molded counterparts. 8SC and 10SC, however, have broader and flatter damping peaks, and each shows a second peak (at ~ 45°C for 8SC and ~ 90°C for 10SC) attributed to soft-segment melting. POMO and PDMO segments are probably insoluble in DMF solvent and separated out during the casting process. These solutions were noticeably cloudy, while the others were clear. DSC traces of these materials seen in Figure 9(d) clearly show crystalline melting peaks very close to those shown in Figure 1 for pure POMO and PDMO.

The position of damping peaks can provide information about the degree of phase separation in PUs. The difference between the T_g of the soft microphase and the T_g of the pure soft segment (i.e., ΔT_g) is an indication of the relative number of hard blocks dissolved in the soft phase. Table III shows the ΔT_g values for the as-molded materials. DMTA tan δ peak temperature values were used for the PU soft microphase T_g values (as opposed to T_g values taken from the DSC thermograms) since the DMTA technique provided more easily distinguishable values. For the POMO- and PDMO-based materials, the soft microphase T_g was extremely difficult to

Table IV Summary of DSC Features for the Molded and Annealed Samples

Material	Soft-phase T_g (°C)	Soft-phase Melting (°C)	Hard-phase T_g (°C)	Hard-phase Melting (°C) (1st, 2nd)	Hard-phase ΔH (Jg^{-1}) (Total 1 + 2)[a]
2M	−20	*	100	188	2.0
4M	−39	*	95	165, 194	10.4
6M	−38	*	90	184	13.8
8M	—	17	95	162, 194	20.7
10M	—	29, 53	93	162, 194	29.1
PCM	22	100[b]	*	*	*
2A120	−23	*	76	186	4.2
4A120	−45	*	61	161, 199	28.2
6A120	−40	*	*	149, 199	32.2
8A120	—	10, 63	*	163, 201	34.7
10A120	—	15	*	143, 195	35.1
PCA120	8	70[b]	*	170	16.7
2A150	−44	*	72	171, 202	17.3
4A150	−40	*	72	171, 202	17.8
6A150	−37	*	70	171, 200	24.4
8A150	—	17	70	180, 202	23.3
10A150	—	32	65	180, 202	31.8
PCA150	20	80[b]	*	*	*

* No transition observed; —, too difficult to distinguish T_g value from the thermogram.

[a] Enthalpy of fusion values for hard-domain melting were calculated "per gram of hard segment" rather than per gram of polymer and comprised the total enthalpy of both melting peaks where dual endotherms were encountered.

[b] These endotherms seen for the PCDO-based polymer were ascribed to "whole chain" crystallinity rather than the "bundle crystallinity" common to the hard and soft microphases.

identify using DSC. It should be noted that the DMTA technique generally provides higher T_g values than does DSC (usually up to 10°C higher) due to the dynamic nature of the test.

PCM stands out as being the most highly phase-mixed material (largest ΔT_g value), while 2M and 4M are the most phase-mixed of the polyether-based materials. Unexpectedly, 6M shows up as having the highest degree of phase separation. A possible explanation for the higher than expected ΔT_g values for 8M and 10M lies in their semicrystalline soft domains (as seen in the DSC thermograms). The presence of such "paracrystalline" soft-phase regions not only causes a higher tan δ peak temperature (compared with what would be seen for a 100% amorphous sample), but may also reduce the volume of the amorphous soft phase in which the stray hard blocks may dissolve, thus further increasing the soft-domain T_g value due to an increase in hard block concentration (in the amorphous fraction).

Figure 8 shows the variations in polymer T_g with annealing. Generally speaking, annealing at 120°C provided better phase separation—hence, purer soft domains and lower soft microphase T_g values. Annealing at 150°C produced a higher soft-domain T_g in all cases, suggesting more phase mixing. Evidence to support this is also seen in the DSC results where the materials annealed at 120°C show greater hard-domain melting enthalpies, as well as less pronounced hard-domain glass transitions than those polymers annealed at 150°C. The fact that the materials annealed at 120°C were annealed for a longer period may have also contributed to these T_g differences.

Differential Scanning Calorimetry (DSC)

Figure 9(a)–(d) shows the DSC thermograms for the as-molded, annealed at 120°C (24 h), annealed at 150°C (10 h), and solvent-cast materials. The characteristic growth and shift of the hard-domain melting endotherms with annealing is observed for the molded and annealed samples. Peak temperatures and enthalpy values are given in Table IV.

Due to their relatively rapid cool from the melt, the as-molded materials show limited hard-domain crystallinity compared to the annealed samples. The molding procedure also resulted in pronounced hard-

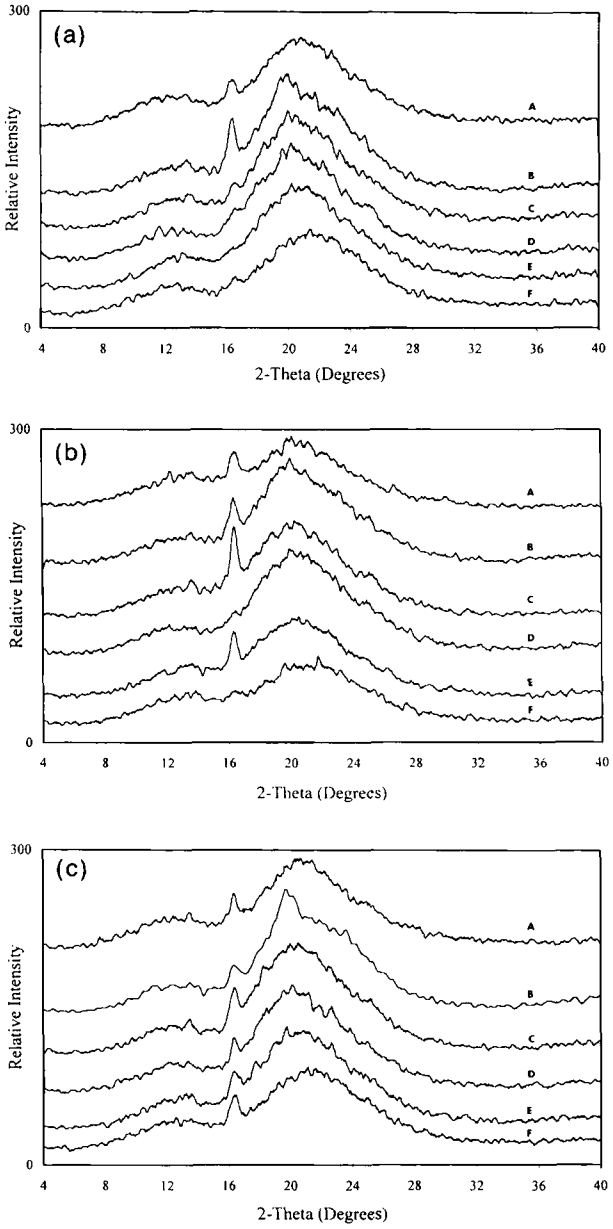

Figure 10 (a) WAXD patterns for the as-molded PUs: (A) PCM; (B) 10M; (C) 8M; (D) 6M; (E) 4M; (F) 2M. (b) WAXD patterns for PUs annealed at 120°C: (A) PCA120; (B) 10A120; (C) 8A120; (D) 6A120; (E) 4A120; (F) 2A120. (c) WAXD patterns for PUs annealed at 150°C: (A) PCA150; (B) 10A150; (C) 8A150; (D) 6A150; (E) 4A150; (F) 2A150.

domain glass transitions (approximately 90–100°C). These hard-domain glass transitions are immediately followed by small endotherms which are believed to be associated with an enthalpy relaxation phenomena. In this process, a type of "partial ordering" of the initially amorphous hard-domain fraction (including the hard–soft interface) occurs during aging at a temperature below the hard microphase T_g.

The corresponding rescan showed no such endotherm because no aging time was allowed for this ordering to take place. The small endotherm common to all thermograms of the PCDO-based material is attributed to "whole chain" ordering, bearing in mind that both the soft and hard segments in this material are capable of hydrogen bonding. The thermograms for 8M and 10M indicate some para-

Table V WAXS Peak Positions for PUs

Material	Diffraction Angles, 2θ	d-Spacings (Å)
2M	16.38	5.41
4M	—	—
6M	16.50	5.37
8M	16.50	5.37
10M	16.38, 19.96, 21.84	5.41, 4.45,[a] 4.07[a]
PCM	16.38	5.41
2A120	16.38	5.41
4A120	16.31	5.43
6A120	16.44, 25.11	5.39, 3.54[b]
8A120	16.38, 25.11	5.41, 3.54[b]
10A120	16.38, 23.23, 25.11	5.41, 3.83,[b] 3.54[b]
PCA120	16.44, 26.68	5.39, 3.34
2A150	16.38	5.41
4A150	16.31	5.43
6A150	16.31	5.43
8A150	16.38	5.41
10A150	16.31, 19.71	5.43, 4.50[b]
PCA150	16.31	5.43

[a] d-Spacing matches with that shown for pure PDMO macrodiol (Table II) and is, hence, attributed to PDMO order.

[b] d-Spacing matches with that shown for the MDI/BDO polymer (Table II) and/or reported WAXD d-spacings for MDI/BDO crystals and is, hence, attributed to hard-segment order.

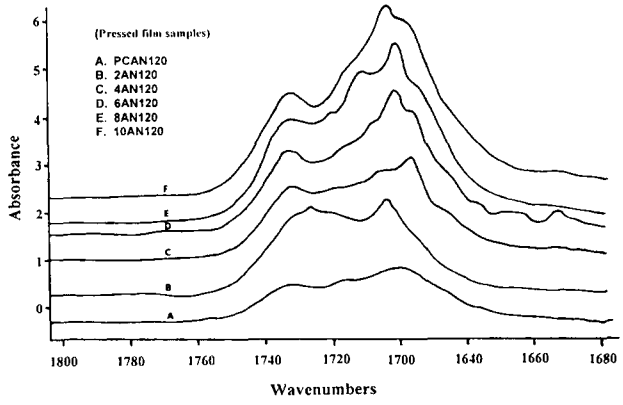

Figure 11 FTIR spectra showing the carbonyl absorbance region for the thin-film samples annealed at 120°C.

Table VI Molecular Weight, Hardness, and Tensile Properties of As-molded Materials

Material	M_n/1000	Shore Hardness (20°C) Shore A	Shore Hardness (20°C) Shore D	UTS (MPa)	Fail Strain (%)	Permanent Set (%)	Stress at 100% Strain (MPa)
2M	177	72	31	19	535	65	5
4M	83	89	45	36	481	69	10
6M	79	91	46	22	442	91	12
8M	114	93	48	39	353	52	16
10M	93	94	55	32	366	86	22
PCM	223	91	61	45	189	20	31

crystallinity in the soft domains (broad endotherms at 20–30°C) and a greater amount of hard domain crystallinity (194°C). 10M also displayed a small crystalline soft-segment peak at 53°C, suggesting a high level of immiscibility between PDMO and MDI/BDO and facilitated also by the rapid crystallizability of PDMO. Broader and less pronounced soft-domain glass transitions accompany the polymers containing the more hydrophobic polyether soft segments (in agreement with the dynamic mechanical behavior).

Annealing promoted ordering in the hard domains. The multiple endothermic behavior observed in the MDI/BDO polymer (Fig. 3) is also seen for the annealed PUs. Several trends develop (Table IV) including an increase in hard-domain crystallinity as the soft-segment CH_2/O ratio (hydrophobicity) increases. Although annealing at 150°C produces higher melting hard domains, it is the 120°C annealing treatment that produces the greatest degree of hard-domain crystallinity (except for 2A120, which shows a quite large, broad cold crystallization exotherm just above the hard-domain T_g). This higher degree of hard-domain crystallinity, together with the absence of hard-domain glass transitions for 6A120, 8A120, and 10A120 materials suggests that this heat treatment results in superior phase separation, with annealing at the higher temperature encouraging the mixing of some of the shorter hard blocks into soft domains and interfacial regions. Furthermore, the A150 materials include quite prominent hard-domain glass transitions.

Interestingly, hard-domain glass transitions for the as-molded samples were higher than those for the annealed (150°C) materials. The as-molded hard-domain T_g's also involved larger ΔCp shifts (as can be seen by the relative scales). This is because annealed materials include less amorphous hard domains than do the as-molded materials; hence, the values seen for the annealed materials are more likely to be a representation of the T_g of the diffuse interfacial regions, incorporating a higher fraction of soft segments than the glassy as-molded hard domains.

Thermograms of the solvent-cast, vacuum-dried samples display obvious differences between the morphologies of molded and cast materials. None of the samples exhibit any significant hard-domain order. The outstanding features include the unusual broad low-temperature endotherm for 2SC (most likely due to some kind of "desolvation process," although this has not been proven) and the very sharp endotherms for 8SC (65°C) and 10SC (80°C) which are undoubtedly due to crystalline POMO and PDMO separating out. As mentioned earlier, the 8 and 10 materials did not dissolve easily in DMF due to the hydrophobicity of the soft segments involved. The 2SC, 4SC, and 6SC materials felt reasonably strong and flexible, whereas the 8SC and 10SC materials had very little mechanical integrity and were very opaque.

Wide-angle X-ray Diffraction (WAXD)

Figure 10(a)–(c) shows the WAXD patterns for molded and annealed samples. Peak positions are given in Table V.

All the diffraction patterns exhibit two broad peaks at approximately 13° and 21°, indicating the existence of short-range ordering. A comparison of these patterns to those of the MDI/BDO copolymer (Fig. 4) confirms that they arise from short-range ordering in the hard domains. For each set of curves, the central broad maximum is seen to shift slightly to lower angles (from 21.5° to 19.7°) with an increase in CH_2/O ratio of the soft segment employed. This is most likely due to an increase in hard-domain order. Also, common to most of the diffraction patterns is the presence of a sharper peak at 5.4 Å *d*-spacing. This peak was present for the MDI/BDO

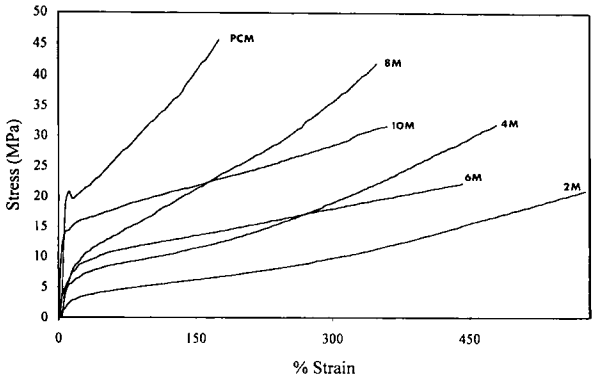

Figure 12 Typical tensile stress–strain curves for the as-molded materials.

polymer sample which had been annealed at 210°C and has been attributed to ordering of single MDI hard segments, as discussed earlier. Support for this argument has been obtained from the WAXD diffraction pattern for an ethanol end-capped MDI compound which also produced the 5.4 Å *d*-spacing. Furthermore, this diffraction peak position has not been seen in the literature. 6A120, 8A120, and 10A120 display very small additional peaks which also match the MDI/BDO (A210) peaks (Table II) and other reported lattice spacings.[3,25–28] 10M displays two small diffraction peaks which compare quite well with values found for pure PDMO (Table II). A PDMO soft-segment melting endotherm was seen in the DSC curve for 10M; hence, it is quite likely that these diffraction peaks are, in fact, due to a small fraction of crystalline PDMO. As mentioned earlier, the peak broadening effect of small crystallites must be considered when looking at semicrystalline polymers.[24]

Fourier Transform Infrared Spectroscopy (FTIR)

Infrared spectroscopy is useful as a morphological probe for PUs since the presence of spectral features can be related to specific aspects of morphology.[33,34] For PUs, the carbonyl absorption region is of particular interest, since it gives information about interurethane hydrogen bonding. Frequency shifts on hydrogen bonding occur for the carbonyl vibration. Participation in hydrogen bonding decreases the non-bonded carbonyl vibration [ν(C=O)free $\sim$ 1730 cm^{-1}] to a lower frequency [ν(C=O)bonded $\sim$ 1700 cm^{-1}]. Since the polyether soft segments contain no proton donor groups, interurethane hydrogen bonding must take place in the hard domains and the relative intensity of the bonded and non-bonded absorbance peaks give us information about the degree of phase separation.

FTIR spectra showing the carbonyl absorbance region for the thin-film samples annealed at 120°C for 24 h are shown in Figure 11. An increase in the soft-segment CH_2/O ratio is accompanied by an increase in the ratio of H-bonded carbonyl groups (right-hand peak) to free carbonyl groups (left-hand peak). This reinforces our DSC findings in showing an increase in phase separation and hard-domain crystallinity as the soft segments employed become more hydrophobic.

Physical Testing

After molding and aging at room temperature for several weeks, the molecular weight, Shore hardness, and tensile properties of each material were determined (Table VI). Table VI summarizes the molecular weights and some of the physical properties of the six materials in the as-molded condition. The molecular weights of all six materials were relatively high, suggesting that the synthesis method was effective. Typical tensile stress–strain curves for these materials are shown in Figure 12.

For the polyether-based materials, an increase in hardness, stiffness (as measured by stress at 100% strain values and DMTA storage modulus [E'] values [Fig. 7]) and opacity were observed for an accompanying increase in the CH_2/O ratio of the soft segment. These differing properties result from two different phenomena: First, the materials are greatly influenced by the properties of the soft segments employed (especially the soft microphase T_g), and, second, the resultant morphology of each material affects its tensile properties. For example, better phase separation and, therefore, a more developed reinforcing hard-domain structure will increase the stiffness of the material and, to an extent, improve its tensile strength. Some phase separation is required to provide enough physical crosslink sites to impart elastomeric behavior. On the other hand, if the hard and soft domains are extremely immiscible, sharp phase boundaries result and a localization of shear stresses can occur, giving rise to poor tensile properties.[35] Also, the ability of the soft segment to crystallize under strain has an inherent effect on the tensile properties. Plaques of 2M appeared transparent; however, 4M, 6M, 8M, and 10M were, respectively, more translucent to opaque in appearance due to an increasing degree of crystallinity. PCM was transparent, yet very stiff and strong, more like a tough thermoplastic than an elastomer. This material displayed the highest tensile strength,

owing to its high concentration of H-bonding sites between both hard and soft blocks and also due to the fact that its soft-domain T_g was above room temperature (34°C, see Table III). The other materials, particularly 2M and 4M, display typical elastomeric stress–strain curves, with high elongations and an upturn in the stress–strain occurring due to stress crystallization of the soft segments. The lesser slope of the 10M curve at high strain compared to the 8M curve may have arisen from the presence of partly crystalline soft domains in 10M, leading to a restriction of the "stress-crystallizability" of these regions. Also, because 10M is highly phase-separated, it is possible that localization of shear stresses (described earlier) occurred at the narrow interface, resulting in a weaker structure. The lower tensile strength observed for 6M may be a result of having the lowest molecular weight value (this was also reflected in a high permanent set).

CONCLUSIONS

This work comprised a systematic study of the effect on morphology and properties of altering the CH_2/O ratio in a series of polyetherurethanes of fixed soft-segment molecular weight and wt % soft segment. The effect on morphology of fabricating by solvent casting as compared to compression molding was also studied, as was the effect of annealing the compression-molded polymers.

The following conclusions were drawn from the study: Increasing the soft-segment CH_2/O ratio decreased the compatibility between the hard and soft segments; hence, an increase in phase separation and hard-domain order was observed. The structure of the hard domains was determined to be predominantly paracrystalline (i.e., ordered without having a repeating unit cell structure).

Soft domains were generally amorphous with POMO and PDMO soft domains exhibiting evidence of paracrystallinity. Exceptions were 10M, 8SC, and 10SC, which displayed small amounts of soft-segment crystallinity. The PCDO-based material displayed the highest degree of phase mixing and was not elastomeric at room temperature.

Increasing the soft-segment CH_2/O ratio caused an increase in stiffness and hardness and a decrease in elongation and clarity. The PCDO-based material was below its soft-domain T_g at room temperature and was, hence, the stiffest and hardest material. It also displayed the highest strength.

Annealing the molded materials increased the hard-domain order, while the as-molded materials had more glassy hard domains. Annealing at 120°C (24 h) provided the greatest phase separation and hard domain melting enthalpy values. Annealing at 150°C (10 h) produced the highest hard-domain melting temperatures. However, it also allowed significant hard–soft segment mixing in the interfacial regions and soft domains.

Solvent casting was difficult for the POMO- and PDMO-based polymers where the soft-segment components were insoluble in the dimethylformamide solvent and separated out to form pure crystalline regions. The resulting materials had poor mechanical properties. PEO-, PTMO-, PHMO-, and PCDO-based materials were more readily solvent-cast and produced films with good mechanical properties. The solvent-cast morphologies were quite different from the morphologies of the molded materials.

The authors wish to acknowledge the assistance Mrs. M. Gertner for her help with the thermal analysis. This work was supported by the CRC for Cardiac Technology and an Australian Postgraduate Research Award.

REFERENCES

1. Z. Ophir and G. L. Wilkes, *J. Polym. Sci. Polym. Phys. Ed.*, **18,** 1469 (1980).
2. Y. Li, Z. Ren, M. Zhao, H. Yang, and B. Chu, *Macromolecules,* **26,** 612 (1993).
3. J. W. C. Van Bogart, P. E. Gibson, and S. L. Cooper, *J. Polym. Sci. Polym. Phys. Ed.*, **21,** 65 (1983).
4. D. S. Huh and S. L. Cooper, *Polym. Eng. Sci.*, **11,** 369 (1971).
5. S. Abouzahr and G. L. Wilkes, *Polymer,* **23,** 1077 (1982).
6. H. N. Ng, A. E. Allegrezza, R. W. Seymour, and S. L. Cooper, *Polymer,* **14,** 255 (1973).
7. W. Chen, K. C. Frisch, D. J. Kenney, and S. Wong, *J.M.S.-Pure Appl. Chem.*, **29,** 567 (1992).
8. Z. S. Petrovic and I. Javni, *J. Polym. Sci. Polym. Phys. Ed.*, **27,** 545 (1989).
9. S. L. Samuels and G. L. Wilkes, *J. Polym. Sci. Polym. Phys. Ed.*, **11,** 807 (1973).
10. L. M. Leung and J. T. Koberstein, *Macromolecules,* **19,** 706 (1986).
11. J. T. Koberstein and T. P. Russell, *Macromolecules,* **19,** 714 (1986).
12. L. M. Leung and J. T. Koberstein, *J. Polym. Sci. Polym. Phys. Ed.*, **23,** 1883 (1985).
13. L. B. Liu, M. Sumita, and K. Miyasaka, *J. Macromol. Sci. Phys.*, **B28,** 309 (1989).
14. M. Shibayama, T. Kawauchi, T. Kotani, S. Nomura, and T. Matsuda, *Polymer,* **18,** 719 (1986).
15. G. L. Wilkes, S. Bagrodia, W. Humphries, and R. Wildnauer, *Polym. Lett.*, **13,** 321 (1975).

16. T. K. Kwei, *J. Appl. Polym. Sci.*, **27,** 2891 (1982).
17. Y. Li, T. Gao and B. Chu, *Macromolecules,* **25,** 1737 (1992).
18. W. Bras, G. E. Derbyshire, G. N. Greaves, G. R. Mant, S. Naylor, and A. J. Ryan, *Mater. Res. Soc. Symp. Proc.,* **307,** 333 (1993).
19. P. A. Gunatillake, G. F. Meijs, R. C. Chatelier, D. M. McIntosh, and E. Rizzardo, *Polym. Int.,* **27,** 275 (1992).
20. D. J. Lyman, *J. Polym. Sci.,* **45,** 49 (1960).
21. G. F. Meijs, P. A. Gunatillake, E. Rizzardo, S. J. McCarthy, and R. C. Chatelier, in *Progress in Pacific Polymer Science 2,* Y. Imanishi, Ed., Springer-Verlag, Berlin, Heidelberg, 1992.
22. P. A. Gunatillake, G. F. Meijs, E. Rizzardo, R. C. Chatelier, S. J. McCarthy, A. Brandwood, and K. Schindhelm, *J. Appl. Polym. Sci.,* **46,** 319 (1992).
23. G. F. Meijs, S. J. McCarthy, E. Rizzardo, Y. Chen, R. C. Chatelier, A. Brandwood, and K. Schindhelm, *J. Biomed. Mater. Res.,* **27,** 345 (1993).
24. B. D. Cullity, *Elements of X-Ray Diffraction,* 2nd ed., Addison-Wesley, Reading, MA, 1978.
25. J. Blackwell and C. D. Lee, *J. Polym. Sci. Polym. Phys. Ed.,* **22,** 759 (1984).
26. L. Born, J. Chrone, H. Hespe, E. H. Muller, and K. H. Wolf, *J. Polym. Sci. Polym. Phys. Ed.,* **22,** 163 (1984).
27. K. S. Hwang, G. Wu, S. B. Lin, and S. L. Cooper, *J. Polym. Sci. Polym. Chem. Ed.,* **22,** 1677 (1984).
28. J. T. Koberstein and A. F. Galambos, *Macromolecules,* **25**(21), 5618 (1992).
29. J. T. Koberstein and R. S. Stein, *J. Polym. Sci. Polym. Phys. Ed.,* **21,** 1439 (1983).
30. Y. Camberlin, J. P. Pascault, M. Letoffe, and P. Claudy, *J. Polym. Sci. Polym. Chem. Ed.,* **20,** 383 (1982).
31. T. Murayama, *Dynamic Mechanical Analysis of Polymeric Materials,* Elsevier, New York, 1978.
32. N. G. McCrum, B. E. Read, and G. Williams, *Anelastic and Dielectric Effects in Polymeric Solids,* Wiley, London, 1967.
33. S. L. Cooper and R. W. Seymour, in *Proceedings of the 19th Sagamore Army Materials Research Conference, 1972,* Syracuse University Press, Syracuse, NY, 1973.
34. R. W. Seymour, G. M. Estes, and S. L. Cooper, *Macromolecules,* **3,** 579 (1970).
35. T. A. Speckhard and S. L. Cooper, *Rubb. Chem. Technol.,* **59,** 405 (1986).

Received September 19, 1995
Accepted October 23, 1995